

## Nuclear structure studies on halo nuclei by direct reactions with radioactive beams

PETER EGELHOF

Gesellschaft für Schwerionenforschung (GSI), D-64291 Darmstadt, Germany

**Abstract.** The investigation of direct reactions with exotic beams in inverse kinematics gives access to a wide field of nuclear structure studies in the region far off stability. The basic concept and the methods involved are briefly discussed. The present contribution will focus on the investigation of light neutron-rich halo nuclei. Such nuclei reveal a new type of nuclear structure, namely an extended neutron distribution surrounding a nuclear core. An overview on this phenomenon, and on the various methods which gave first evidence and qualitative confirmation of our present picture of halo nuclei, is given.

To obtain more quantitative information on the radial shape of halo nuclei, elastic proton scattering on neutron-rich light nuclei at intermediate energies was recently investigated for the first time. This method is demonstrated to be an effective means for studying the nuclear matter distributions of such nuclei. The results on the nuclear matter radii of  ${}^6\text{He}$  and  ${}^8\text{He}$ , the deduced nuclear matter density distributions, and the significance of the data on the halo structure is discussed. The present data allow also a sensitive test of theoretical model calculations on the structure of neutron-rich helium isotopes. A few examples are presented.

The investigation of few-nucleon transfer reactions in inverse kinematics may provide new and complementary information on nuclear structure, as well as astrophysical questions. The physics motivation and the experimental concept for such experiments, to be performed due to momentum matching reasons at low incident energies around 5 – 20 MeV/u at the new generation low energy radioactive beam facilities SPIRAL, PIAFE, etc., is briefly discussed.

**Keywords.** Halo nuclei; direct reactions with radioactive beams; nuclear matter radii.

**PACS Nos** 21.10.Gv; 25.40.Cm; 25.60.-t; 25.60.Dz; 25.60.Gc; 27.20.+n

### 1. Introduction

One of the most powerful classical methods for obtaining spectroscopic information on the structure of nuclei is the investigation of light-ion induced direct reactions, i.e. elastic or inelastic scattering, or one- and few-nucleon transfer reactions. A lot of what we know about the structure of stable nuclei was obtained from such investigations. Of course, before the availability of radioactive ion beams, this method was limited to stable or very long-lived nuclei for which targets could be prepared. The use of good-quality secondary exotic beams now enables to study such reactions on exotic nuclei using the method of inverse kinematics, which is sketched in figure 1 for the example of a  $(d, p)$  reaction.

In principle, a large variety of light-ion induced reactions with various physics motivations may be investigated. One- and few-nucleon transfer reactions, such as  $(d, p)$ ,  $(p, d)$ ,

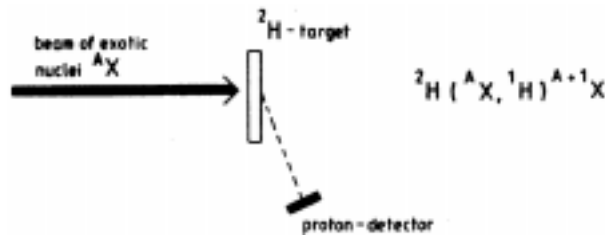


**Figure 1.** The method of inverse kinematics is sketched for the example of a  $(d, p)$ -reaction on the nucleus  ${}^A X$ .

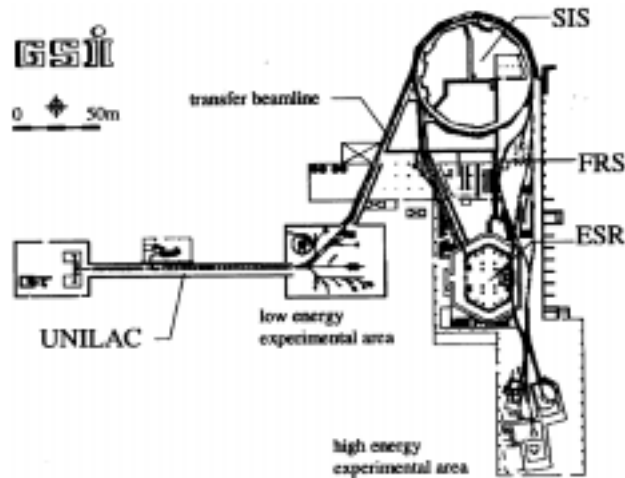


**Figure 2.** Schematic view of the accelerator facilities at GSI, Darmstadt. Heavy-ion beams of all ion species up to  ${}^{238}\text{U}$  from the linear accelerator UNILAC ( $E \leq 20$  MeV/u) are post-accelerated by the heavy-ion synchrotron SIS ( $E \leq 2$  GeV/u), and may be injected into the fragment separator FRS and (or) into the experimental storage ring ESR.

$(d, t)$ ,  $(d, {}^3\text{He})$ ,  $({}^3\text{He}, \alpha)$ , etc., allow to populate single-particle (hole) states or two-particle (two-hole) states, whereas inelastic  $(p, p')$ ,  $(\alpha, \alpha')$ , etc. scattering leads to the population of collective states, and  $(p, p)$ ,  $(\alpha, \alpha)$ , etc. elastic scattering allows to deduce information on the nuclear matter distribution of nuclei. Of particular physics interest are, for example, the nuclear shell model in the region far off stability, the two-body residual interaction in nuclei, as well as astrophysical questions, transition densities and deformation parameters, the radial shape of nuclei, etc.

The new heavy-ion accelerator facilities at GSI Darmstadt (see figure 2), which came into operation in 1990, opened new opportunities for a variety of nuclear physics studies. With respect to exotic nuclei the combination of the heavy-ion synchrotron SIS, the fragment separator FRS and, for selected cases, the experimental storage ring ESR provides good-quality beams of relatively short-lived nuclei, extending to isotopes far off stability, in the energy range from the Coulomb barrier up to intermediate energies around 1 GeV/u.

The present contribution will focus on nuclear structure studies on light neutron-rich halo nuclei. Such nuclei, located near or at the neutron drip line, in particular  ${}^6\text{He}$ ,  ${}^8\text{He}$ ,  ${}^{11}\text{Li}$ ,  ${}^{14}\text{Be}$ , etc., have attracted much attention in the recent years since there is clear experimental evidence that these nuclei reveal a qualitatively new type of nuclear structure, namely an extended neutron distribution surrounding a nuclear core.

A brief overview on this phenomenon and on some of the experimental methods which gave first evidence, and which were used for further experimental access to the halo structure of nuclei, is given in the following section. The third section is dedicated to the investigation of nuclear matter distributions of halo nuclei by intermediate-energy elastic proton scattering, a method which was applied on exotic nuclei for the first time in recent experiments at GSI. Finally, the investigation of few-nucleon transfer reactions in inverse kinematics is discussed which may in future provide complementary information on the structure of halo nuclei.

## 2. Halo nuclei – A new phenomenon of the structure of nuclei

The discovery and the interpretation of the phenomenon of halo nuclei was initiated in the mid-eighties by the pioneering work of Tanihata and coworkers [1–3]. In these experiments the total interaction cross section  $\sigma_I$  was determined for the interaction of light neutron-rich isotopes with various targets.  $\sigma_I$  was deduced from the change of intensity of a beam of exotic nuclei before and after hitting a target. From the measured interaction cross sections the nuclear matter radii  $R_I(\text{proj.})$  of the projectile nuclei may be estimated by simple geometrical considerations using the relation

$$\sigma_I = \pi[R_I(\text{proj.}) + R_I(\text{tar.})]^2, \quad (1)$$

$R_I(\text{tar.})$  being the matter radius of the target nucleus (it should be noted that for a quantitative determination of the matter radii a more sophisticated analysis taking into account the reaction dynamics was used).

The surprisingly steep rise of  $\sigma_I$  for  ${}^{11}\text{Li}$  in the chain of the Li-isotopes, and less pronounced, for  ${}^6\text{He}$  and  ${}^8\text{He}$  for the He-isotopes, was therefore interpreted as due to a pronounced increase of the nuclear matter radius. In figure 3 a compilation of such data [3] measured for a larger number of neutron-rich isotopes is displayed. In almost all of the isotope chains we observe for the most neutron-rich nuclei a deviation from the  $A^{(1/3)}$ -law (see dotted line in figure 3), which is well established for stable and less exotic nuclei. These findings were at that time interpreted in terms of the following picture (see also figure 4): For the case of ‘normal’ nuclei, which are stable or are situated close to the valley of stability, and which therefore possess only a small excess of neutrons, the neutrons and protons are equally distributed (left part of figure 4), and the addition of one neutron will not drastically change the spatial extension of the nucleus. In contrast, a new phenomenon of nuclear structure appears for some nuclei which are close to the drip line, and for which the binding energy of additional valence nuclei is consequently very low, usually of the order of a few hundred keV only. Adding one or more neutrons to such an already very neutron-rich nucleus will produce in certain cases a so-called ‘halo’ around a nuclear core, consisting of an extremely spatially extended, low-density aureole in which the additional neutrons are located (right part of figure 4). Thus, in special cases, a significant

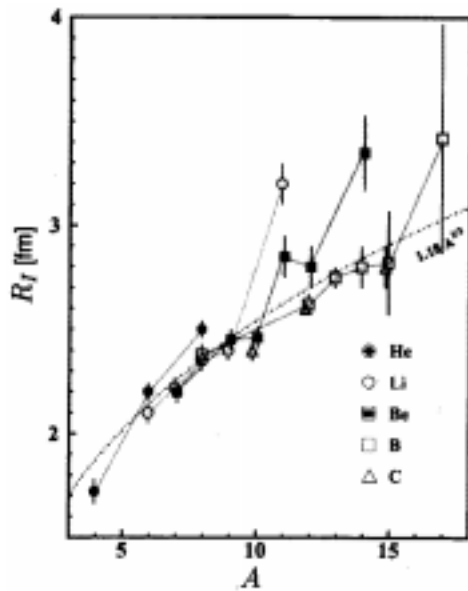


**Figure 3.** Nuclear matter radii  $R_I$  deduced from measured total interaction cross sections for several isotope chains of light neutron-rich nuclei (from ref. [3]).

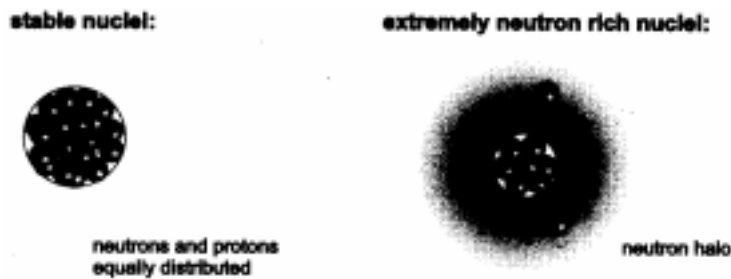


**Figure 4.** Density distributions of nuclear matter for stable nuclei and extremely neutron-rich nuclei.

fraction of more than 90% of the valence neutron wave function can be outside the central part of the nucleus, leading to an extended radius of the nuclear matter distribution. So, for example, the nuclear radius determined for  $^{11}\text{Li}$  is similar to that of the stable  $^{32}\text{S}$ , which consists of approximately three times the number of nucleons. It turns out that the phenomenon of halo nuclei is always closely connected to a very low binding energy of the valence nucleons.

In order to confirm the present picture of halo nuclei, and to get a deeper insight into the structure of such nuclei, halo nuclei were subjected to numerous studies during the last decade, using various methods. For a detailed overview over this field the reader may be referred to recent review articles [4–7]. Experiments performed at the on-line mass separator ISOLDE at CERN focused on the electric and magnetic moments of halo nuclei

[8,9]. Beta-decay measurements following in-beam polarization by optical pumping on  $^9\text{Li}$  and  $^{11}\text{Li}$  showed that the electric and magnetic properties of both nuclei are very similar. This finding is a clear confirmation that the large interaction cross section obtained for  $^{11}\text{Li}$  is only due to the spatial distribution of the valence neutrons, and not created by core deformation or core polarization effects.

Another frequently used method is the investigation of momentum distributions of the reaction products after fragmentation of the halo nucleus following the interaction with a target. Experiments were performed using beams produced by heavy ion projectile fragmentation and in-flight separation at GANIL, MSU, RIKEN in the energy range 20–80 MeV/u, and at BEVALAC and GSI for higher incident energies of about 200–1000 MeV/u. Thus, a large variety of data on longitudinal and transverse momentum distributions of the heavy ‘core’-fragment, and of the valence neutrons, and, in kinematically complete experiments, of both have been taken for various exotic nuclei, and for various targets and incident energies (for an overview see [4–7,10], and references therein).

It follows from relatively simple considerations that the momentum distributions of the fragments reflect the intrinsic distribution of the constituents, and thus the spatial structure of the fragmenting nucleus. The momentum distribution of the valence neutrons of the nucleus being the Fourier transform of its wave function, the size of the spatial distribution of the nucleus is – due to the uncertainty principle – expected to be inversely proportional to the width  $\Gamma$  of the momentum distribution. Hence we obtain for the root mean square matter radius:

$$\langle R_m^2 \rangle^{1/2} \sim 1/\Gamma. \quad (2)$$

Indeed, narrow momentum distributions were obtained for practically all candidates for halo nuclei, as established from the data on the total interaction cross section. As an example, recent data [11] on longitudinal momentum distributions of  $^{18}\text{C}$  ( $^{16}\text{C}$ )-fragments after one-neutron removal from  $^{19}\text{C}$  ( $^{17}\text{C}$ )-projectiles are displayed in figure 5. Both projectile nuclei are assumed to have an extended neutron distribution due to the small binding energy of the valence neutron. Consequently both momentum distributions are found to be narrower by factors of about 2 and 3 compared to the corresponding momentum

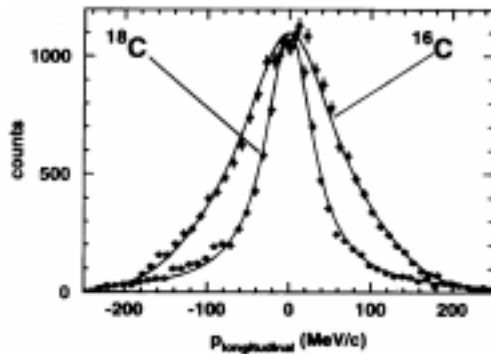


**Figure 5.** Longitudinal momentum distributions of  $^{18}\text{C}$ , and  $^{16}\text{C}$  after one-neutron removal from  $^{19}\text{C}$ , and  $^{17}\text{C}$ , respectively (from ref. [11]).

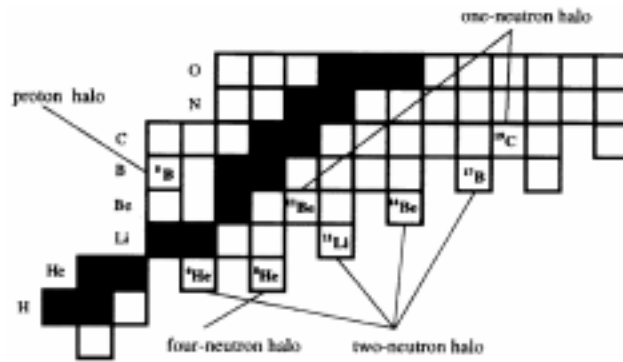


**Figure 6.** Chart of isotopes up to element  $Z = 8$ . Nuclei for which a halo structure was confirmed experimentally are indicated.

distributions of tightly bound nuclei, thus confirming an extended neutron distribution in both nuclei. The significant difference in the width of the distributions is attributed to the difference in the separation energies of the valence neutron, and thus a pronounced halo structure is established for the  $^{19}\text{C}$  nucleus. Figure 6 displays the latest compilation of nuclei for which the halo structure has been confirmed by the various experimental information. Besides one-, two-, and four-neutron halos on the neutron-rich side, there is meanwhile also evidence for proton halos.

In summary we conclude that the assumed picture on the structure of halo nuclei, established after the finding of the large interaction radii (see above), was qualitatively confirmed by various experiments. Halo nuclei are thus characterized by large interaction cross sections, weak binding of the valence nucleon(s), and narrow momentum distributions of the reaction products after fragmentation. On the other hand it should be pointed out, that a more quantitative information on the radial structure and the size of halo nuclei from such experiments is to a considerable extent limited by the limited knowledge of the underlying reaction mechanism and dynamics of the reactions used. Hence, systematic uncertainties in the determination of the matter radii appear due to uncertainties created by effects like the interaction of the target with the nuclear constituents, by the final state interaction of the knocked-out fragments with the remaining system, etc.. Thus, in order to obtain more quantitative information on the radial shape of halo nuclei and the nuclear matter radii, the method of elastic proton scattering at intermediate energy was recently applied, as will be discussed in the following section.

### 3. Nuclear matter distributions of halo nuclei from elastic proton scattering at intermediate energy

Proton nucleus elastic scattering at intermediate energies was proved (for the case of stable nuclei) to be a well suited method for obtaining accurate and detailed information on nuclear matter distributions of nuclei [12]. This method was recently applied at GSI Darmstadt for the first time for the investigation of exotic nuclei. The advantage of such experiments as compared to investigations at considerably lower incident energies (see for example [13,14]) is, that for intermediate energies, available for exotic beams at GSI,

proton-nucleus elastic scattering can be described accurately by the diffractive multiple scattering theory which relates the measured cross section to the nuclear matter distribution in a rather unambiguous way [12]. Furthermore, as theoretical considerations have shown [15,16], proton scattering in the region of small momentum transfer is sensitive to the halo structure of nuclei. Thus, besides the precise determination of the nuclear matter radius, information on the shape of the radial distribution of nuclear matter of halo nuclei can be obtained. Both quantities are fundamental quantities of nuclei, and therefore of large interest for our understanding of the structure of halo nuclei, and for an effective test of respective theoretical model calculations.

Differential cross sections for elastic proton scattering at small scattering angles were measured at GSI Darmstadt at energies around 700 MeV/u in inverse kinematics for the neutron-rich helium isotopes  $^6\text{He}$ ,  $^8\text{He}$  [17,18], and recently also for the neutron-rich lithium isotopes  $^8\text{Li}$ ,  $^9\text{Li}$ , and  $^{11}\text{Li}$ . The present contribution will mainly concentrate on data on the helium isotopes for which the data analysis was completed recently [16]. Secondary  $^{4,6,8}\text{He}$  beams (the  $p$   $^4\text{He}$  cross section was measured for a consistency check of the method) were produced with incident energies of 699 MeV/u, 717 MeV/u, and 674 MeV/u, respectively, by fragmentation of  $^{18}\text{O}$  ions from the heavy-ion synchrotron SIS (see figure 2), impinging on a beryllium target, and were isotopically separated by the fragment separator FRS [19]. The separation method is displayed schematically in figure 7 for the production of a  $^6\text{He}$  beam as an example. In the first section of the FRS the produced isotopes are separated according to their magnetic rigidity, resulting in a selection

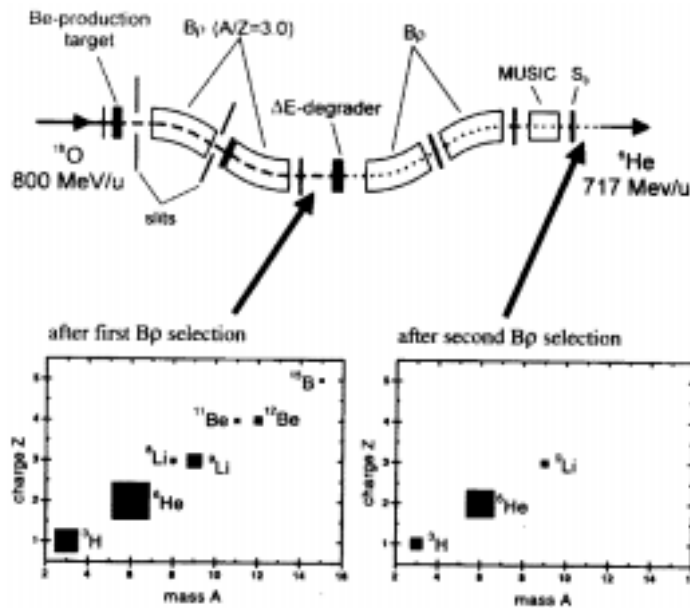


**Figure 7.** The operation principle of the fragment separator FRS is displayed for the example of the separation of a  $^6\text{He}$  beam after bombardment of a Be production target with a  $^{18}\text{O}$  beam (upper part). The resulting isotope distributions after the first and the second  $B\rho$  selection are shown in the lower part of the figure.

of all isotopes with  $A/Z \approx 3.0$  (see lower part of figure 7). The separation power was considerably enhanced by inserting an achromatic energy degrader at the dispersive focal plane. The thickness of the degrader in terms of the range of the beam particles was about 0.05, resulting in a rather clean  ${}^6\text{He}$  beam after the second separator stage. The intensity of the secondary beams was about  $10^3 \text{ sec}^{-1}$  in all cases.

The experimental setup is displayed in figure 8 (for more details on the technical design and experimental procedure see also refs [18,20]). The relatively low secondary beam intensities for isotopes close to the drip line demand for a thick effective hydrogen target, and for a large solid angle detector for the recoil protons. In order to meet these experimental conditions the hydrogen filled time-projection ionization chamber IKAR was used, which serves simultaneously as a gas target and a detector. It was developed at the St. Petersburg Nuclear Physics Institute (PNPI), Gatchina, and was originally used for studying small angle hadron elastic scattering [21]. IKAR ensures a high  $\text{H}_2$  target thickness (about  $3 \times 10^{22} \text{ protons/cm}^2$ ), and has a  $2\pi$  acceptance in azimuthal angle for recoil proton registration. It operates at 10 bar pressure of hydrogen and consists of 6 identical modules. One of these modules is shown schematically in figure 9, together with an illustration of a typical scattering event between a projectile nucleus and a proton from the chamber gas. Each module contains an anode plate, divided into two rings (A and B), a cathode plate and a grid, the whole setup being rotationally symmetric with respect to the beam axis. The amplitude and the drift time analysis of the signals from the electrodes, registered by flash ADCs, provide the energy  $T_R$  of the recoil proton, or its energy loss  $\Delta T_R$  in case it leaves the active volume, the scattering angle  $\Theta_R$  of the recoil proton, and the coordinate  $z$  of the interaction point in the grid-cathode space. The obtained energy and angular resolutions are  $\Delta E \leq 90 \text{ keV}$ , and  $\Delta \Theta_R \leq 0.6^\circ$ , respectively, and the coordinate  $z$  is determined with an accuracy of  $\Delta z \leq 100 \mu\text{m}$ . The detector is able to operate at secondary beam intensities up to about  $10^4 \text{ sec}^{-1}$ . The scattering angle  $\Theta_s$  for the helium projectiles was determined by a tracking detector consisting of 4 two-dimensional multiwire-proportional chambers (see figure 8). In addition, the scintillation counters S1, S2, S3, and VETO were

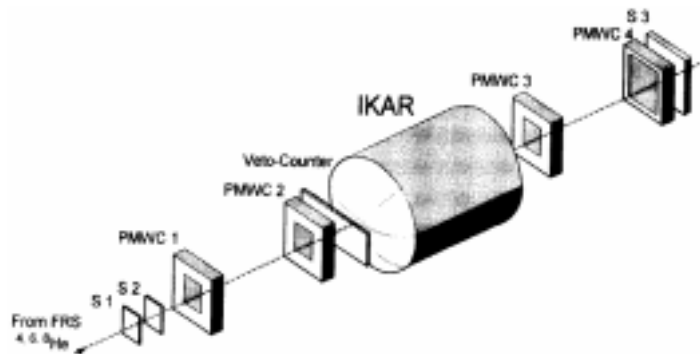


**Figure 8.** Schematic view of the experimental setup. The central part shows the hydrogen filled ionization chamber IKAR which serves simultaneously as a gas target and a detector system for recoil protons. Four multiwire proportional chambers (PMWC 1-4) determine the scattering angle of the projectile. Scintillation counters (S1-S3, VETO) were used for trigger and for particle identification.

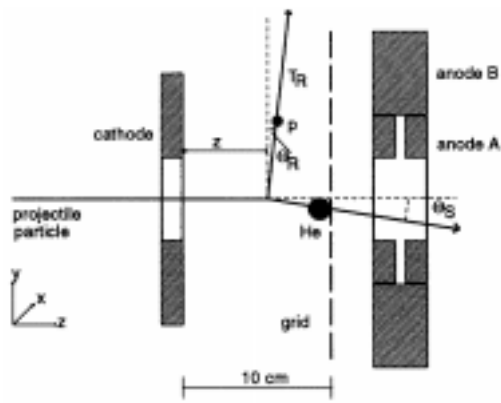


Figure 9. Schematic view of one of the six ionization chamber modules of IKAR.

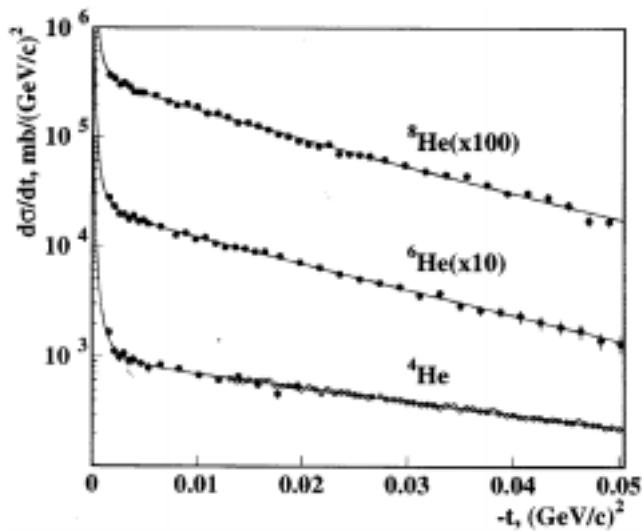


Figure 10. Absolute differential cross sections  $d\sigma/dt$  versus the four momentum transfer squared  $-t$  for  $p^4\text{He}$ ,  $p^6\text{He}$  and  $p^8\text{He}$  elastic scattering at incident energies of 699 MeV/u, 717 MeV/u, and 674 MeV/u, respectively, obtained from the present experiment (full dots). Open dots show the data of ref. [22]. Full lines are the result of fits using the GH parametrization for the nuclear density distributions.

used for triggering, and for the identification of the incident and scattered beam particles via time-of-flight and  $dE/dx$  measurements.

The resulting cross sections are displayed in figure 10. Plotted error bars denote statistical errors only. The absolute normalization obtained is estimated to be accurate within  $\pm 3\%$ . The measured  $p^4\text{He}$  cross section is in excellent agreement with previous data [22], which were obtained in direct kinematics.

To derive information on the nuclear density distributions of  ${}^6\text{He}$  and  ${}^8\text{He}$  from the measured cross sections the Glauber multiple scattering theory was applied. Calculations were performed using the basic Glauber formula [12] for proton–nucleus elastic scattering, and taking experimental data on proton–proton and proton–neutron scattering as an input. For the analysis of the present experiment [16,17] various parametrizations of the nuclear density distributions of  ${}^4\text{He}$ ,  ${}^6\text{He}$  and  ${}^8\text{He}$  were used as an input for the Glauber calculations, and the parameters were varied in order to obtain a best fit to the experimental cross sections. All nucleon distributions deduced, as well as the resulting root mean square radii  $R_m$ , refer to point nucleon distributions. Two parametrizations of the total matter distribution  $\rho_m(r)$  were used which do not make a difference between core and valence nucleons, namely a symmetrized Fermi (SF) distribution, and a Gaussian with a ‘halo’ (GH) (for details see ref. [16]). Furthermore two parametrizations were applied which assume that the  ${}^{6,8}\text{He}$  nuclei consist of an  $\alpha$  core and of 2(4) valence neutrons for  ${}^6\text{He}$  ( ${}^8\text{He}$ ). Here, a Gaussian distribution for the core, and either a Gaussian (GG) or a  $1p$ -shell harmonic oscillator-type density (GO) for the valence neutrons were used.

The experimental data are equally well described independent of the density parametrization used, with a reduced  $\chi^2$  around unity. Solid lines in figure 10 show the GH case as an example. The deduced nuclear matter density distributions  $\rho_m(r)$  for  ${}^6\text{He}$  and  ${}^8\text{He}$  are displayed in figure 11 in comparison with the one for  ${}^4\text{He}$ . The results for all four parametrizations used agree reasonably well within small errors (for a detailed discussion see ref. [16]) over a wide range of the radius parameter  $r$ . For both neutron-rich He isotopes,  ${}^6\text{He}$  and  ${}^8\text{He}$ , rather extended matter distributions were obtained, the matter densities decreasing much slower with the radius than the one for  ${}^4\text{He}$ . This result is interpreted as a clear evidence for the existence of a significant neutron halo in  ${}^6\text{He}$  and  ${}^8\text{He}$ .

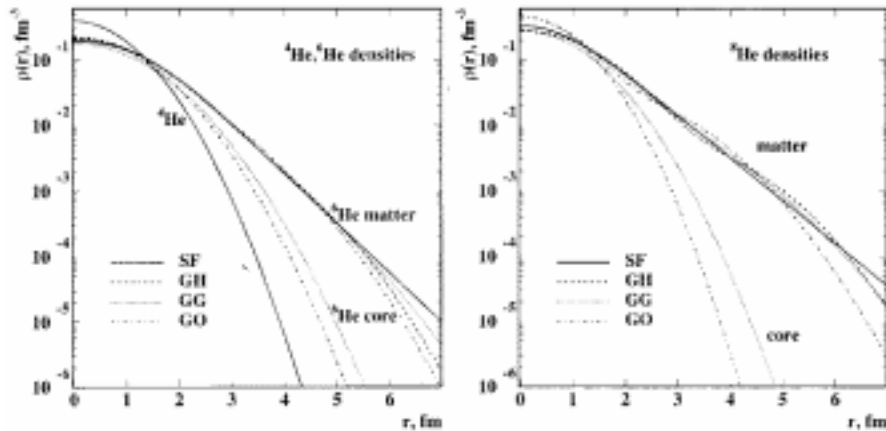


**Figure 11.** Nuclear core and nuclear matter density distributions  $\rho(r)$  for  ${}^6\text{He}$  (left side) and for  ${}^8\text{He}$  (right side) obtained for the different parametrizations applied (for notations see text). For a comparison the nuclear matter density distribution for  ${}^4\text{He}$  is also plotted (left side). Curves are normalized to the number of nucleons.

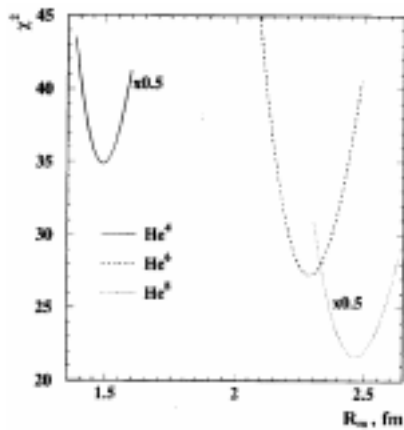


**Figure 12.**  $\chi^2$  values versus the matter radius  $R_m$ , obtained from a fit to the data for  ${}^4\text{He}$ ,  ${}^6\text{He}$  and  ${}^8\text{He}$  using the parametrization GH.

To demonstrate the sensitivity of the data on the matter radius  $R_m$  the  $\chi^2$  dependence of the fitting parameter  $R_m$  is displayed in figure 12 for the example of the analysis with the parametrization GH. Both parametrizations (SF and GH) applied for  ${}^4\text{He}$  have yielded identical values  $R_m = 1.49 \pm 0.03$  fm. In the case of  ${}^6\text{He}$  and  ${}^8\text{He}$  the values obtained for the matter radii  $R_m$  from the four parametrizations mutually agree within small errors ( $\pm 0.02$  fm). This demonstrates that the results of the radii are quite independent of the model assumptions considered. The final average values are  $R_m = 2.30 \pm 0.07$  fm for  ${}^6\text{He}$ , and  $R_m = 2.45 \pm 0.07$  fm for  ${}^8\text{He}$  (with total errors including systematical uncertainties). The values determined for the core radii are  $R_c = 1.88 \pm 0.12$  fm for  ${}^6\text{He}$ , and  $R_c = 1.55 \pm 0.15$  fm for  ${}^8\text{He}$ .

The present data on nuclear matter radii from elastic proton scattering cross sections may be compared to corresponding data deduced from the total interaction cross sections, a method which was discussed in §2 of this contribution. Such a comparison is of special interest, as both methods to determine nuclear matter radii are independent. The results from the present experiment are in close agreement with the accepted values  $R_m = 2.33 \pm 0.04$  fm for  ${}^6\text{He}$  and  $R_m = 2.49 \pm 0.04$  fm for  ${}^8\text{He}$  from Tanihata *et al* [25]. However, the data on the  ${}^6\text{He}$  matter radius from the total interaction cross sections were again under discussion recently, as a re-analysis [26,27] of the data from ref. [2] resulted in two new values for  $R_m$ , which both disagree with the radius from the present experiment. In figure 13 the results on the matter radius of  ${}^6\text{He}$  from various analysis [23–27] over the years, which were all based on the same experimental data set from Tanihata *et al* [2], are displayed (black dots). For comparison the result of the present experiment is also shown in figure 13 (open square). It may be concluded from figure 13 that the error bars given for the various values deduced from analysing the data on the total interaction cross section do in some cases not include, or underestimate the systematical uncertainties. At present this topic is still under discussion.

Besides the determination of phenomenological nucleon density distributions and their parameters, the present data allow also a sensitive test of theoretical model calculations on the structure of neutron-rich nuclei. As an example, the results of microscopic calculations performed in the framework of the refined resonating group model (RRGM) [28], using as

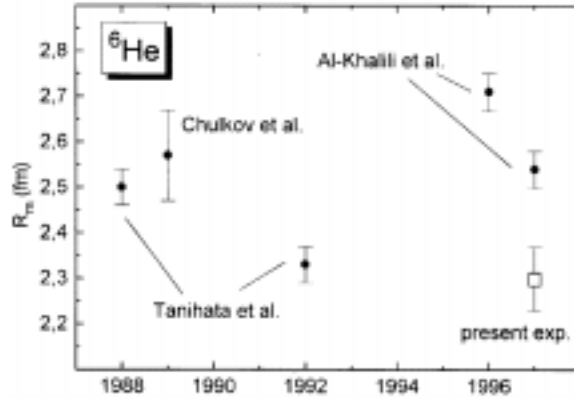


**Figure 13.** Compilation of values for the nuclear matter radius of  ${}^6\text{He}$ , deduced from various analysis [23–27], which were all based on the same data set on the total interaction cross sections [2] (black dots). For comparison the value obtained from the present experiment is also shown (open square).

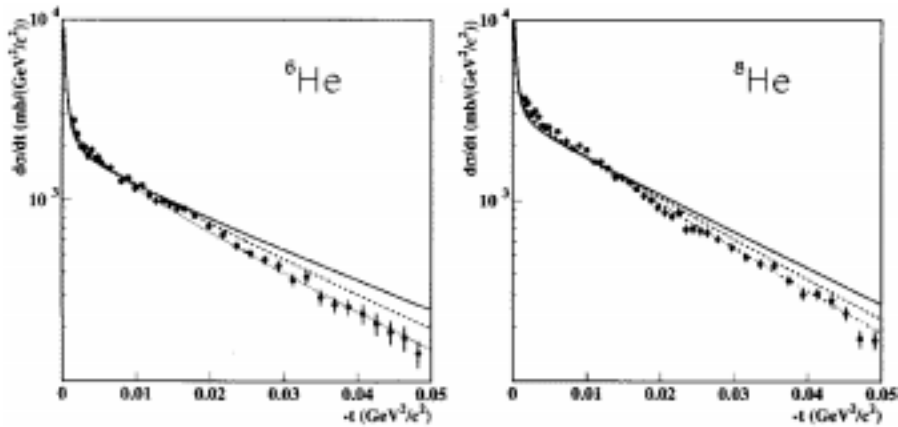


**Figure 14.** Differential cross sections for  $p{}^6\text{He}$  scattering (left side) and  $p{}^8\text{He}$  scattering (right side) obtained from the present experiment are compared with calculated cross sections on the basis of nuclear matter distributions resulting from microscopic RRGm calculations with various effective nucleon–nucleon forces, namely CS (solid lines), SZ (dashed lines), SZ-V2 (dotted line), modified SZ-V2 (dashed-dotted line). For notations see text.

an input various effective nucleon–nucleon forces without additional free parameters, are compared with the experimental data. For that purpose, the nucleon density distributions obtained from the theoretical RRGm calculations [29,30] for the different helium isotopes investigated were used as an input for Glauber calculations, as described above. Finally the obtained ‘theoretical cross sections’ were compared with the experimental data, thus allowing for a test of the nucleon–nucleon force used. In figure 14 the experimental data

on  ${}^6\text{He}$  and  ${}^8\text{He}$  are displayed in comparison with the corresponding results of RRGm calculations [29,30] performed with the effective nucleon–nucleon force introduced by Csoto (CS), and various modifications of the effective nucleon–nucleon force introduced by Stöwe and Zahn (SZ) (for details see refs [20,29,30]). For both isotopes, the SZ-V2 force, which includes (as compared to the original version SZ-2) the central force in the odd-parity singlet and triplet states of the nucleon–nucleon two-body force, yields the best description of the experimental data. In the case of  ${}^8\text{He}$  the SZ-V2 force had to be modified [30] (inclusion of a realistic hard core) to obtain a reasonable agreement with the experimental data.

In figure 15 (left side) the corresponding theoretical nuclear matter density distributions are, for the case of  ${}^6\text{He}$ , compared with the distribution deduced from the present experiment for the GG parametrization (see above). For  $r < 5$  fm, the best agreement is obtained for the SZ-V2 force which gave also the best agreement for the cross sections. There seems to be a general trend of these calculations to exhibit, as compared to the experimental result, an enhanced tail for very large radii ( $r > 5$  fm). This trend is in agreement with calculations from ref. [26], but in disagreement with a recent calculation using the boson dynamic-correlation model [31]. The result of this calculation is also shown in figure 15 (right side). A remarkably good agreement with the experimentally determined density distribution over the whole range of the radius parameter  $r$  is obtained.

In an experiment performed very recently at GSI Darmstadt data on elastic proton scattering from neutron-rich lithium isotopes  ${}^8\text{Li}$ ,  ${}^9\text{Li}$  and  ${}^{11}\text{Li}$  were taken using the same experimental method. At present the data analysis is in progress. From the statistics

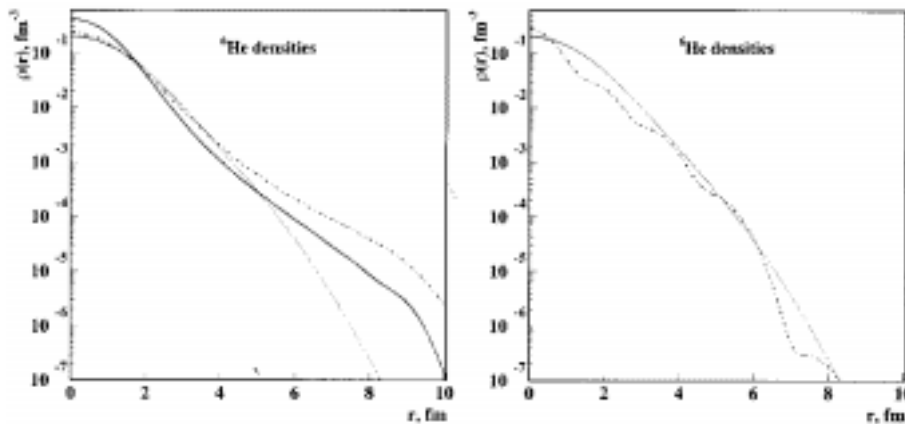


**Figure 15.** On the left side the nuclear matter density distribution for  ${}^6\text{He}$ , obtained from microscopic RRGm calculations with the effective nucleon–nucleon forces CS (solid line) and SZ-V2 (dashed-dotted line), are compared with the density distribution deduced from the present experiment for the GG parametrization (dotted line). On the right side of the figure, again the distribution deduced from the present experiment (dotted line) is compared with the result of a calculation using the boson dynamic-correlation model [31] (dashed-dotted line).

obtained we expect a similar, or even better sensitivity on the nuclear matter distributions of  $^8,9,11\text{Li}$  as compared to the case of the helium isotopes.

#### 4. Investigation of few-nucleon transfer reactions

The investigation of light ion induced few-nucleon transfer reactions with exotic beams in inverse kinematics opens potentially a large spectrum of physics interest. The experimental scenario for such measurements is essentially different from the one for elastic and inelastic scattering. This is mainly due to the fact that incident energies of the order of 5 – 20 MeV/u are required to fulfill the momentum matching criterion for the transferred particle(s). For much higher energies the momentum mismatch for the transferred nucleon in projectile and target will lead to a loss of cross section and  $l$ -selectivity, the latter needed for an unambiguous identification of the populated states. Such experiments are most favourably performed at the new generation of radioactive beam facilities presently under construction or just starting operation (for example: SPIRAL at GANIL, France, REX-ISOLDE at CERN, Switzerland, or PIAFE at Munich, Germany, etc.), which provide good quality low energy exotic beams. Therefore the present contribution mainly concentrates on the future perspectives and possibilities (for a more detailed discussion of this topic see also [32]).

The investigation of few-nucleon transfer reactions (for example  $(d, p)$ ,  $(p, d)$ ,  $(p, t)$ , etc.) allows the population and spectroscopy of single particle- and single hole-states, as well as two particle (hole)-states, which is of particular interest in the region near closed shells. The location and identification of such states and the determination of their spectroscopic strength provides a sensitive test of the nuclear shell model in the region far off stability. It should be pointed out, that such studies are complementary to decay spectroscopy, which does not allow to determine spectroscopic factors. The investigation of two particle (hole)-states in the vicinity of doubly closed-shell nuclei opens the possibility to deduce matrix elements of the two-body residual interaction, which is an important input for microscopic calculations. Many new combinations of shell model orbits become available by investigating nuclei near the doubly magic  $^{132}\text{Sn}$  nucleus. Moreover the spectroscopy (identification of energy levels and determination of spectroscopic factors) of neutron resonances by the  $(d, p)$ -reaction on  $r$ -process nuclei in the  $A \approx 80$  and  $A \approx 130$  regions (near the neutron shell-closures) may yield important data, necessary to explain the observed solar isotopic abundance pattern and to give constraints on neutron density and temperature for the astrophysical scenario.

With respect to neutron-rich light halo nuclei information on neutron pair-correlations may be obtained from the comparison of cross sections for one- and two-neutron pickup reactions, whereas neutron-stripping reactions may allow spectroscopy at or even beyond the drip line.

As the intensities of secondary exotic beams are limited, all these experiments require thick effective targets and large solid angle detector systems. Therefore we propose to use the concept of a time-projection ionization chamber as active target, similar to the one discussed in §3, also for experiments with low-energy exotic beams. Of course such a design has to be adjusted to the specific experimental conditions. In figure 16 a design for such a device is displayed together with the experimental situation for the example of a  $(p, t)$  reaction on  $^{11}\text{Li}$ . Due to the relatively high specific energy loss of the beam particles in the entrance window, its thickness, and therefore the operating pressure, has

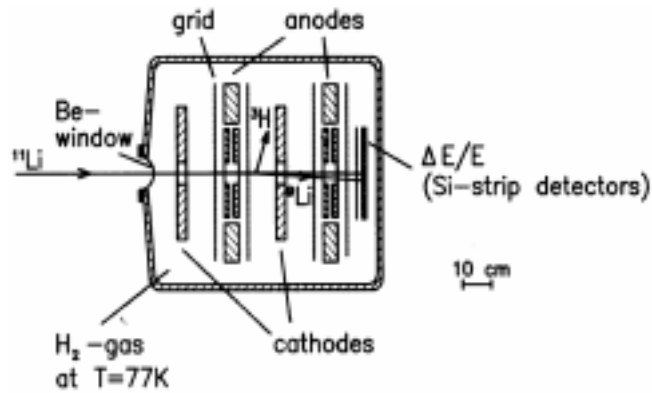


**Figure 16.** Schematic view of a design for a time-projection ionization chamber as active target for the investigation of direct reactions with exotic beams at low incident energies around 5–20 MeV/u.

to be limited to about 1–2 bar. In order to ensure sufficient target thickness and stopping power to stop the target like particles, the whole setup is operated at LN<sub>2</sub> temperature. The operating principle and the readout procedure will be similar to that discussed in §3 (see also figure 9). In summary, such a device will provide a high target thickness up to 10–20 mg/cm<sup>2</sup> of pure hydrogen, a large detector solid angle (angular acceptance: 20° < Θ < 160° over the whole azimuthal angle), and good energy and angular resolution (see §3). Particle identification is provided by ΔE/E techniques due to a separated anode (for the target-like particles), and a forward ΔE/E silicon strip telescope (for the projectile-like particles). This setup may be used for all kinds of direct reactions with low energy secondary beams and with H<sub>2</sub>, D<sub>2</sub>, <sup>3</sup>He, <sup>4</sup>He targets. Due to the increase of energy loss in the entrance window and the gas for very heavy ions its application will be limited to light beams up to Z ≈ 15 – 20.

For experiments with heavier beams more conventional setups using large solid angle arrays of silicon strip detectors or PIN-diodes and solid targets (for example CH<sub>n</sub>, CD<sub>n</sub> or deuterated Ti-foils) may be used. It has been demonstrated in a prototype experiment [33], where the d(<sup>136</sup>Xe, p)<sup>137</sup>Xe\* reaction was investigated at E = 5.9 MeV/u with stable beam in inverse kinematics, that such an experimental setup will be well suited, and will provide sufficient energy resolution (ΔE < 80 keV) for such measurements with exotic beams.

For the identification of heavy projectile-like reaction products in the outgoing channel the concept of calorimetric low temperature detectors provides considerable advantage over conventional detection schemes, and is therefore foreseen, for example, for the VAMOS spectrometer, presently under construction for the SPIRAL facility at GANIL, France. For such detectors, operated at temperatures around T ≈ 1.5–2 K, excellent energy resolutions of ΔE/E ≈ 1 – 2 · 10<sup>-3</sup> were achieved [34,35] even for very heavy ions like <sup>238</sup>U. Thus their use for the isotope mass identification via a TOF/energy measurement may allow the separation of masses up to the heaviest isotopes, and replace the standard TOF/B · ρ method with solid angle limiting magnet spectrometers.

## Acknowledgements

The author is indebted to G D Alkhazov, M Mutterer and S R Neumaier for many stimulating discussions, and to W Falkenberg for the help in preparing the manuscript.

## References

- [1] I Tanihata *et al*, *Phys. Rev. Lett.* **55**, 2676 (1985)
- [2] I Tanihata *et al*, *Phys. Lett.* **B160**, 380 (1985)
- [3] I Tanihata, *Nucl. Phys.* **A488**, 113c (1988)
- [4] K Riisager, *Rev. Mod. Phys.* **66**, 1105 (1994)
- [5] P G Hansen *et al*, *Ann. Rev. Nucl. Part. Sci.* **45**, 591 (1995)
- [6] I Tanihata, *Prog. Part. Nucl. Phys.* **35**, 505 (1995)
- [7] I Tanihata, *J. Phys.* **G22**, 157 (1996)
- [8] E Arnold *et al*, *Phys. Lett.* **B197**, 311 (1987)
- [9] E Arnold *et al*, *Phys. Lett.* **B281**, 16 (1992)
- [10] H Emling, *J. Phys.* **G24**, 1561 (1998)
- [11] T Baumann *et al*, *Phys. Lett.* **B439**, 256 (1998)
- [12] G D Alkhazov *et al*, *Phys. Rep.* **42**, 89 (1978)
- [13] A A Korshennikov *et al*, *Nucl. Phys.* **A617**, 45 (1997)
- [14] M D Cortina-Gil *et al*, *Phys. Lett.* **B401**, 9 (1997)
- [15] G D Alkhazov *et al*, *Pisma ZhETF* **55**, 377 (1992); *JETP Lett.* **55**, 379 (1992)
- [16] G D Alkhazov *et al*, *Nucl. Phys.* (1999) to be published
- [17] G D Alkhazov *et al*, *Phys. Rev. Lett.* **78**, 2313 (1997)
- [18] S R Neumaier *et al*, *Nucl. Phys.* (1999) to be published
- [19] H Geissel *et al*, *Nucl. Instr. Meth.* **B70**, 286 (1992)
- [20] S R Neumaier *et al*, Proc. Int. Conf. on Exotic Nuclei and Atomic Masses, ENAM, Arles, France, *Edit. Front.* **227** (1995)
- [21] A A Vorobyov *et al*, *Nucl. Instr. Meth.* **119**, 509 (1974)
- [22] O G Grebenjuk *et al*, *Nucl. Phys.* **A500**, 637 (1989)
- [23] I Tanihata *et al*, *Phys. Lett.* **B206**, 592 (1988)
- [24] L V Chulkov *et al*, *Europhys. Lett.* **8**, 245 (1989)
- [25] I Tanihata *et al*, *Phys. Lett.* **B289**, 261 (1992)
- [26] J S Al-Khalili *et al*, *Phys. Rev.* **C54**, 1843 (1996)
- [27] J S Al-Khalili *et al*, *Nucl. Phys.* **A616**, 418c (1997)
- [28] H M Hofmann, *Lecture Notes in Physics* **273**, 243 (1987)
- [29] J Wurzer *et al*, *Phys. Rev.* **C55**, 688 (1997) and references therein
- [30] J Wurzer, PhD thesis, University of Erlangen (1997)
- [31] M Tomaselli *et al*, (1999) to be published: GSI scientific report 1998
- [32] P Egelhof, *Proc. of the Int. Workshop on Research with Fission Fragments*, Benediktbeuren, 1996, World Scientific, ISBN 981-02-3140-7, p. 178 (1997)
- [33] G Kraus *et al*, *Z. Phys.* **A340**, 339 (1991)
- [34] A V Kienlin *et al*, *Nucl. Instr. Meth.* **A368**, 815 (1996)
- [35] H J Meier *et al*, *Nucl. Phys.* **A626**, 451c (1997)